NUMERICAL ANALYSIS OF NEXT ION THRUSTER OPTICS

Jerold W. Emhoff, Graduate Student Research Assistant
Iain D. Boyd, Professor
Steven P. Shepard, Undergraduate Student
Department of Aerospace Engineering
University of Michigan, Ann Arbor, MI 48109

Abstract

Results from several different computational studies of the NEXT ion thruster optics are presented. The dependence of accelerator grid current on downstream domain length is explored. It is found that the current increases continually with domain length and a possible method for improvement is suggested. A study on the effect of beam voltage on accelerator grid aperture wall erosion shows a non-monotonic, complex behavior. Comparison to experimental performance data indicates improvements in simulation of the accelerator grid current, as well as very good agreement with other quantities. Also examined is the effect of ion optics choice on the thruster life, showing that TAG optics provide better margin against electron backstreaming than NSTAR optics. Life estimates are performed for both cusped and non-cusped geometry, indicating that cusped geometry gives lower and most likely more accurate life estimates.

Introduction

The success of the NSTAR ion thruster in the Deep Space One mission[1] has led NASA to develop a new thruster based on NSTAR technology. The aim is to design a thruster with higher thrust, better efficiency, and longer life than the NSTAR thruster, enabling even longer and more ambitious missions than Deep Space One. NASA's Evolutionary Xenon Thruster[2], or NEXT, is a 40 cm thruster, giving approximately twice as much beam extraction area as NSTAR's 30 cm beam diameter. Also, as shown in Soulas et al[3], a redesigned discharge chamber gives a much flatter beam current density profile. The larger beam diameter and flatter beam profile combine to provide more thrust, while reducing the amount of ion optics erosion. Higher beam voltages are also used in the NEXT thruster, giving greater efficiencies than those seen in the NSTAR thruster. The ion optics geometry is largely the same as in the NSTAR thruster, although two optics sets with different accelerator grid thicknesses are under consideration. The first optics set, referred to as the NSTAR optics, has the same accelerator grid thickness as in the NSTAR thruster. The second optics set has an accelerator grid with 50% greater thickness than NSTAR, called the Thick-Accelerator-Grid (TAG) optics[4].

Ion optics modeling is being conducted to aid in the design process of the NEXT thruster. Determining the life of an ion thruster is a difficult, costly, and lengthy process experimentally. As an alternative, modeling can give order of magnitude or better life estimates in a relatively short time, and at a low cost. This has special relevance in the case of NEXT, as the consideration of two accelerator grid geometries makes experimental testing even more complex and expensive.

The focus of this paper is on modeling of the NEXT thruster ion optics, considering both NSTAR and TAG accelerator grids. Simulation data from various thruster operating points and with varying simulation parameters are analyzed. A study is presented where the length of the computational domain downstream of the ion optics is varied to observe the effect on accelerator grid current. Life estimates and performance results are presented for the maximum operating condition of the NEXT thruster, considering differences between the inclusion of cusped geometry and its omission. Performance changes with varying beam voltage are also analyzed and compared to experimental data.

Model Operation

The computational code provides a 2-D axisymmetric simulation of a single aperture in an ion thruster. The grid used is composed of evenly spaced rectangular cells. The optics of the thruster are simulated using boundary cells in the domain. These cells may be arranged in an irregular way, allowing the simulation of cusps on the barrels of the grids. A typical computational domain is shown in Figure 1.

The code uses the Particle-In-Cell[5] (PIC) method to simulate xenon ions, xenon neutrals, and doubly-charged xenon ions. Each computational particle has a numerical weight which indicates the actual number of atoms represented by the particle. Flow field quantities for each cell are obtained by averaging the properties of all the particles in the cell, taking into account the weight of each particle. The potential field accelerates ions self-consistently. Electrons are modeled as a fluid, and the Poisson equation is solved using the Alternating Direct Implicit (ADI) method. Electron densities are retrieved from the potential using the Boltzmann relation. The direct simulation Monte Carlo (DSMC) method[6] is used for processing particle collisions. Both charge exchange and momentum exchange collision types are simulated.

To run a simulation, the beamlet current and mass flow rate must first be determined. This is performed by running short simulations with approximately 3 mm computational domain length downstream of the optics, and no included back pressure. This allows relatively quick determination of the necessary input ion and neutral densities. Once the correct densities are determined, the downstream domain length is increased to approximately 2 cm, and back pressure effects are included. The effect of tank or back pressure is modeled by injection of neutral Xenon at the downstream boundary. No ions are injected at the downstream boundary.

The simulation begins by operating at a large time-step with only neutral particles in the domain. This allows the slow moving neutrals to rapidly reach a steady state flow. Once a steady-state is reached, ions are injected at the upstream boundary with the Bohm velocity and the input density corresponding to the desired beamlet current. At this point, the time-step is decreased so that the ions are not able to cross more than one cell boundary in a single iteration, maintaining stability.

A typical simulation has approximately 800,000 particles. About 180,000 of these are singly charged ions and 600,000 are neutrals. There are also on the order of ten thousand doubly charged ions. For a typical domain size, about 18,000 iterations are needed to initialize the neutral particle flow, followed by approximately 60,000 iterations to initialize the mixed ion-neutral flow before sampling begins. Once a steady flow has been reached, data is sampled from the simulation over a large number of time-steps, typically on the order of 100,000. On a 1.5 GHz Pentium IV PC, a typical simulation has a running time of approximately two days.

Simulation Results

Three sets of simulation data are presented here. First, data obtained by varying the length of the computational domain downstream of the ion optics is analyzed. Next, aperture wall erosion is examined at two operating points, and the effect of cusps is noted. Finally, results are presented for varying beam voltages at the beam current of 3.1 A and compared to experimental results.

Effect of the Computational Domain Length Downstream of the Optics

In this set of computational results, the same operating point is modeled using several different computational domain lengths downstream of the accelerator grid. The purpose is to determine at which point no additional charge-exchange (CEX) ions are collected on the accelerator grid, if such a point exists. All results are at the operating point of 3.1 A, 1750 V beam voltage, assuming a tank pressure of 8 μTorr. NSTAR optics are used in all simulations, but cusps are not modeled. Figure 2 shows the effect of the domain length on the current collected on the downstream face and barrel of the accelerator grid. As expected, the current on the downstream face increases monotonically with increasing domain length, while there is no effect on the barrel current. There is no indication in the plot of a limiting point at which current on the downstream face no longer increases, while it is known that such a point must exist in the actual system.

The source of the problem is the specular reflection boundary condition used at the outer radius of the computational domain. While the actual thruster plume expands downstream of the optics, the specular boundary condition acts to force the beamlet into an artificial tube with constant radius. The result is that the ion density in the downstream region never drops, also preventing the potential from dropping. Without a potential drop in the downstream region, there is no barrier to keep CEX ions from being drawn into the accelerator grid downstream face, and without a decrease in ion and neutral densities, the CEX collision rates remain constant instead of decreasing. Thus, the accelerator current will continue to increase with domain length, no matter how

much the length is increased. One solution to this problem is to give the upper boundary a coefficient of diffusion such that some ions and neutrals are able to escape through the boundary. This coefficient needs to coincide with the expansion of the thruster's plume in order to obtain the correct ion densities. Implementing this change is planned as part of the future work for the model.

For the remainder of this paper, the downstream domain length is arbitrarily set to 2 cm. It is shown above that this length is not sufficient to collect all possible CEX ions on the accelerator grid. However, until modifications are made to the model, no length will be sufficient. So, a length of 2 cm is chosen for consistency, and because it provides enough accelerator grid current to give reasonable comparison to experimental measurements.

Accelerator Grid Wall Erosion Study

Two of the primary failure modes of an ion thruster are electron backstreaming due to enlargement of the accelerator grid aperture and structural failure of the optics due to erosion on the downstream surface of the accelerator grid. A 2-D simulation cannot capture the nuances of the structural failure mode however, so the aperture wall erosion is the main focus here. Two operating points are considered: A total beam current of 3.52 A at a beam voltage of 1800 V, and a total beam current of 3.1 A at 1750 V. These points are used because they are two of the operating points for the NEXT thruster. In all simulations, the beamlet at the center of the optics is modeled, assuming the peak beamlet current for the corresponding total beam current. This gives a beamlet current of about 0.168 mA for the 3.1 A case, and 0.186 mA for the 3.52 A case. Also, both NSTAR and TAG optics are simulated for each operating point. For the 3.1 A cases, no cusps are simulated, but the aperture diameter is varied over several runs to obtain the erosion rate on the accelerator grid aperture wall as the diameter of the aperture increases over the lifetime of the thruster. For the 3.52 A cases, simulation data is given for runs both with and without the cusped geometry. Table 1 summarizes the erosion rates for each operating condition.

To determine the electron backstreaming behavior of the optics, several shortened simulations are performed. In these simulations, no neutrals are included and the domain length downstream of the accelerator grid is maintained at 3 mm. The accelerator grid aperture diameter is varied in each simulation, giving a minimum centerline potential for each configuration. The ion densities injected at the upstream boundary are not changed, so there is some variation in beamlet current. The minimum centerline potential determines whether or not electron backstreaming occurs. If this potential is nearly the same as the downstream plasma potential, electrons can then easily flow into the discharge chamber. This destroys the performance of the thruster. The downstream plasma potential is measured experimentally. Using the erosion rates obtained from the full simulations, the accelerator grid aperture radius can be determined as a function of time. This is then combined with the data for centerline potential and the mass flow rate at the operating point to determine what mass of xenon gas the thruster can process before electron backstreaming occurs.

Figure 3 shows the data for the 3.1 A case in terms of total propellant mass throughput for the thruster, where 5 V is the downstream plasma potential. Even though the erosion rate on the barrel of the TAG optics is twice that of the NSTAR optics at beginning-of-life, the TAG optics have a much longer life. This is partially because the TAG optics have more area to erode on the aperture wall, but also because the added thickness of the grid gives more margin against electron backstreaming. In Figure 4, the aperture wall erosion rate is plotted as a function of accelerator aperture radius for both sets of optics. Although the TAG optics have a much higher erosion rate early in life, the rate drops more quickly, so that after the radius increases by about 26% the erosion rate for both sets of optics is comparable. These results indicate a strong advantage to the use of TAG optics in the NEXT thruster.

Note that the erosion rate increases for both sets of optics early in life as the radius increases, before dropping later in life. This is counter-intuitive, as it is expected that the erosion rate would decrease monotonically as the aperture diameter increases. What likely occurs is that, early in the life of the thruster, the slightly increased diameter allows the barrel of the accelerator grid to collect high energy CEX ions that form upstream of the accelerator grid. At beginning of life, these ions are most likely accelerated through the optics without impinging on any surface. When the diameter increases slightly, the focusing changes such that the high energy

CEX ions are more likely to impinge on the barrel. Then, as the diameter increases further, the neutral density in the discharge chamber decreases due to the widened aperture. This leads to decreased CEX production rates and lower erosion rates on the barrel. Figures 5 and 6 show the change in electric potential as the aperture enlarges for the NSTAR and TAG optics, respectively. The top halves of each plot represent the electric potential contours at beginning-of-life, while the bottom half shows the potential after the aperture diameter has enlarged via erosion. For both sets of optics, the zero-potential contour inside the accelerator grid aperture becomes much more sloped in the downstream direction as the aperture enlarges. Since ions will cross this contour perpendicularly, there is a much greater chance that high energy CEX ions from the upstream region will impact on the accelerator grid barrel. However, the enlarged aperture also provides a larger neutral atom flow area, decreasing the neutral density and the CEX collision rate.

For the 3.52 A cases, the erosion rate is only computed at the beginning of life, so the radius as a function of mass throughput is extrapolated from that initial value. Figure 7 shows the electron backstreaming comparison between the two sets of optics, with and without cusps. The downstream plasma potential in these cases is 22 V, so that is the critical value for the minimum centerline potential. The plot shows that TAG optics again have the advantage over the NSTAR optics, but in both cases, the cusped case performs more poorly. This is because when cusps are not modeled, the life prediction is artificially increased due to added grid material. The grids are modeled as rectangular with the same radius as in the cusped case, so there is additional material surrounding where the cusps should be. As a result, both sets of data where cusps are not included show throughput capabilities of 100 kg or more higher than the cases where cusps are modeled. However, the cusped cases have lower initial erosion rates than the non-cusped cases, so the difference between them decreases as time goes on.

Beam Voltage Study

For much of the NEXT erosion study, it is assumed that the worst case operating point is at the highest beam voltage and the highest beam current. However, it has been postulated by Brophy et al[7] that it may in fact be the case that the perveance fraction is the true determining factor for maximum erosion rate. The perveance fraction is defined as $f_p = \frac{j_b l_e^2}{V_T^{3/2} P_{\max}}$, where $l_e = \sqrt{\left(l_g + t_s\right)^2 + \frac{1}{4} d_s^2}$ and $P_{\max} = \frac{4\varepsilon_0}{9}\left(\frac{2e}{m_i}\right)^{1/2}$. V_T is the beam voltage minus the accelerator grid voltage, j_b is the current density upstream of the optics, l_g is the distance between the grids, t_s is the thickness of the screen grid, d_s is the diameter of the screen grid aperture, e is the electric charge, m_i is the ion mass, and ε_0 is the permittivity of free space. For Xenon, P_{max}=4.77x10^{-9} A/V$^{3/2}$. Results given by Brophy indicate that there is a minimum point for the ion energy impacting on the accelerator grid barrel, and thus a minimum for the erosion rate, at a perveance fraction of about 0.2. Directly above or below this point, the erosion rate rises sharply; in the higher perveance region, a slight drop is seen in the erosion rate. If this is correct, then the most critical operating point would be at the beam voltage and beam current just above the perveance fraction of 0.2. To test this theory, results from five cases modeled in the NEXT thruster are presented. The 3.1 A beam current operating point at beam voltages of 1800 V, 1567 V, 1396 V, and 1179 V are all simulated using both NSTAR and TAG optics. Also, the 2.7 A beam current, 1021 V beam voltage operating point is modeled. At each operating point, the peak beamlet current is simulated. This is 0.168 mA for the 3.1 A cases, and 0.149 mA for the 2.70 A case.

In Figure 8, the erosion rate on the accelerator grid aperture wall as a function of perveance fraction is shown. There is indeed a peak in the erosion rate as the perveance increases beyond 0.2, however, there is a sharper drop following the increase, so that the 2.70 A case at 1021 V still has a lower erosion rate than the 3.1 A, 1800 V case. The TAG optics are less sensitive to the perveance for low values, but then drop more sharply as the perveance increases than the NSTAR optics. Although the peak erosion rate is just above a perveance fraction of 0.2 as Brophy predicts, the rise from 0.2 is much less dramatic, and the drop in erosion rate as the perveance continues to increase is much more severe than predicted by Brophy. This may be a result of the different models used, or because of differences in the operating conditions simulated. In either case, it seems that determining which operating conditions give the worst case erosion rate is non-trivial. Upon closer examination of the determining factors, this makes sense. The accelerator grid barrel erosion rate is caused by both the energy and the amount of impacting CEX ions. The energy is directly related to the beam voltage, so decreasing

the voltage decreases the energy of the CEX ions. However, decreasing the voltage also increases the perveance, so that CEX ions are more likely to be focused onto the aperture wall. This indicates that the worst case erosion will occur at some middle point, where the energy and number of CEX ions combine to give the maximum erosion rate. Both the simulations performed here, and the results given by Brophy confirm this.

Comparison to Experimental Results

Experimental data collected by Soulas et al[8] give the performance of the NEXT thruster at various operating points. Table 2 shows the operating points for the experimental data, taken using the NSTAR optics, as well as the data of interest. The simulated data is evaluated at the peak beamlet for a given operating point, while the experimental data represents the entire thruster. To offset this difference, all simulated results are multiplied by the number of apertures in the thruster, and by the ratio of the peak beamlet current to the average beamlet current. All of the simulated data correspond to the points in the beam voltage study, except for one additional point at a beam current of 3.52 A, with 1800 V beam voltage.

Figure 9 shows the accelerator grid current as a function of beam voltage. The computational results are somewhat lower than the experimental results, although the fact that they are on the same order of magnitude is an improvement over previous results[9]. Some of the difference is from the estimation of the average current from the peak current, but the treatment of the computational domain downstream of the optics is also a factor. The model does predict the change in accelerator current with changing beam current fairly well. The jump from the 2.70 A first point on the plot to the 3.1 A second point is approximately the same for both experimental and simulation results. Also, the model predicts the jump in accelerator current seen at the last point, for the 3.52 A, 1800 V beam voltage operating condition. However, the experimental results show a steady increase in accelerator grid current as the beam voltage increases, and this is not seen in the simulation data. This may be because the cusped geometry is not modeled here, or it may possibly be an effect of differences between the modeled operating point and the experimental, such as varying double ion content.

The thrust as a function of beam voltage is shown in Figure 10. Here, the model follows the exact same trend as the experimental data—a linear increase in thrust as the beam voltage increases, as well as increasing thrust with beam current. The underprediction of the thrust is almost certainly due to the usage of only the peak beamlet. Also shown in Figure 10 is a plot of the model results increased by 15%. These results are almost exactly the same as the experimental results at every point. From this, it is concluded that the comparison to thrust is excellent.

The specific impulse for both experiment and model are shown in Figure 11 as a function of beam voltage. Both sets of data increase linearly with beam voltage. The model results have a slightly different slope however. This may be an effect of using the peak beamlet, or possibly other factors such as double ion fraction. Even so, the comparison to experimental data is very good.

Conclusion

Results from several computational studies were presented in this paper. It was found that increasing the simulated domain length downstream of the ion optics increased the accelerator grid current, and that it continued to do so regardless of how much the domain was lengthened. The outer boundary of the computational domain can be given a coefficient of diffusion to correct this problem. A study of the erosion of the accelerator grid aperture wall showed that the TAG optics allowed more propellant mass throughput before electron backstreaming occurred than the NSTAR optics. This was despite the increased erosion rate on the TAG optics, because the thicker grid gave more area to erode and also provided more margin against electron backstreaming than the thinner NSTAR optics. It was also seen that including cusped geometry on the optics gave lower mass throughput estimates, even though the erosion rates were lower.

No clear relation was apparent between the erosion and either beam voltage or perveance fraction. While it was seen that the highest beam voltage may not give the highest erosion rate, the lowest beam voltage at a given beam current does not necessarily do so either. Comparison to experimental data was good: the simulation of accelerator grid current has improved, and comparisons to thrust and specific impulse were excellent.

Acknowledgement

This work was funded in part by the NASA Glenn Research Center under grant NAG3-2497 with George Soulas as the technical monitor.

References

[1] Polk, J. E., Brinza, D., Kakuda, R. Y., Brophy, J. R., Katz, I., Anderson, J. R., Rawlin, V. K., Patterson, M. J., Sovey, J., Hamley, J., "Demonstration of the NSTAR Ion Propulsion System on the Deep Space One Mission," IEPC-01-075, October 2001.

[2] Patterson, M. J., Foster, J. E., Haag, T. W., Rawlin, V. K., Soulas, G. C., Roman, R. F., "NEXT: NASA's Evolutionary Xenon Thruster," AIAA 2002-3832, July 2002.

[3] Soulas, G. C., Haag, T. W., Patterson, M. J., "Performance Evaluation of 40 cm Ion Optics for the NEXT Ion Engine," AIAA Paper 2002-3834, July 2002.

[4] Soulas, G. C., "Improving the Total Impulse Capability of the NSTAR Ion Thruster with Thick-Accelerator-Grid Ion Optics," IEPC-01-081, October 2001.

[5] Birdsall, C. K. and Langdon, A. B., *Plasma Physics Via Computer Simulation*, Adam Hilger Press, 1991.

[6] Bird, G. A., *Molecular Gas Dynamics and the Direct Simulation of Gas Flows*, Oxford University Press, 1994.

[7] Brophy, J. R., Katz, I., Polk, J. E., Anderson, J. R., "Numerical Simulations of Ion Thruster Accelerator Grid Erosion," AIAA Paper 2002-4261, July 2002.

[8] Personal communication, George Soulas, December 2002.

[9] Emhoff, J. W., Boyd, I. D., "A Numerical Study of Neutralization and Sputtering Processes in the NSTAR Thruster," AIAA Paper 2002-4259, July 2002.

Table 1. Erosion rates and accelerator grid currents at simulated points.

Beam Current (A)	Optics Set	Cusped Geometry	r/r_0	Accelerator Grid Erosion Rates (mg/khr)		Accelerator Grid Current (A)	
				Barrel	Downstream Face	Barrel	Downstream Face
3.1	NSTAR	No	1.00	0.18	0.50	8.03E-08	3.20E-07
3.1	NSTAR	No	1.05	0.22	0.64	9.63E-08	4.02E-07
3.1	NSTAR	No	1.12	0.28	0.62	1.22E-07	3.88E-07
3.1	NSTAR	No	1.19	0.20	0.71	1.27E-07	4.36E-07
3.1	NSTAR	No	1.26	0.19	0.62	1.25E-07	3.72E-07
3.1	NSTAR	No	1.33	0.25	0.57	1.70E-07	3.44E-07
3.1	TAG	No	1.00	0.37	0.50	1.51E-07	3.09E-07
3.1	TAG	No	1.05	0.46	0.57	1.91E-07	3.50E-07
3.1	TAG	No	1.12	0.40	0.65	1.78E-07	4.05E-07
3.1	TAG	No	1.19	0.33	0.66	1.72E-07	4.17E-07
3.1	TAG	No	1.26	0.23	0.57	1.31E-07	3.68E-07
3.1	TAG	No	1.33	0.23	0.63	1.60E-07	3.87E-07
3.1	TAG	No	1.40	0.27	0.62	1.96E-07	3.87E-07
3.52	NSTAR	No	1.00	0.26	0.62	1.04E-07	4.02E-07
3.52	NSTAR	Yes	1.00	0.19	0.64	9.61E-08	4.02E-07
3.52	TAG	No	1.00	0.56	0.56	2.24E-07	3.46E-07
3.52	TAG	Yes	1.00	0.32	0.49	1.41E-07	3.02E-07

Table 2. Operating points and data for comparing the model results to experiment. Computational results shown here are multiplied by the number of apertures and the peak-to-average current ratio.

Beam Current (A)		2.7	3.1	3.1	3.1	3.1	3.52
Beam Voltage (V)		1021	1179	1396	1567	1800	1800
Peak-to-Average Current Ratio		0.61	0.62	0.62	0.62	0.62	0.64
Experimental Results	Accelerator Current (mA)	9.48	11.54	11.69	11.86	12.22	13.51
	Thrust (mN)	71.81	81.42	126.52	182.89	192.23	169.42
	Specific Impulse (s)	3202.27	3631.03	3708.14	4074.49	3341.67	3318.18
Computational Results	Accelerator Current (mA)	7.25	9.11	8.87	7.92	7.17	9.62
	Thrust (mN)	121.98	149.12	162.72	171.10	181.90	207.45
	Specific Impulse (s)	3092.18	3296.82	3566.41	3775.97	4006.24	4020.66

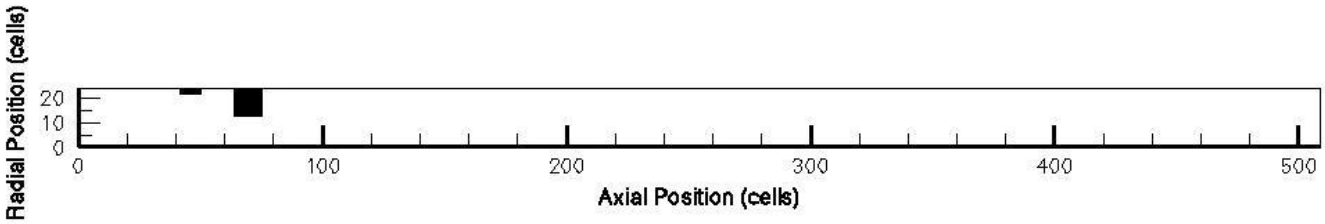

Figure 1. A typical computational domain. The axis numbers represent the number of cells in each direction, and the black areas represent the ion optics.

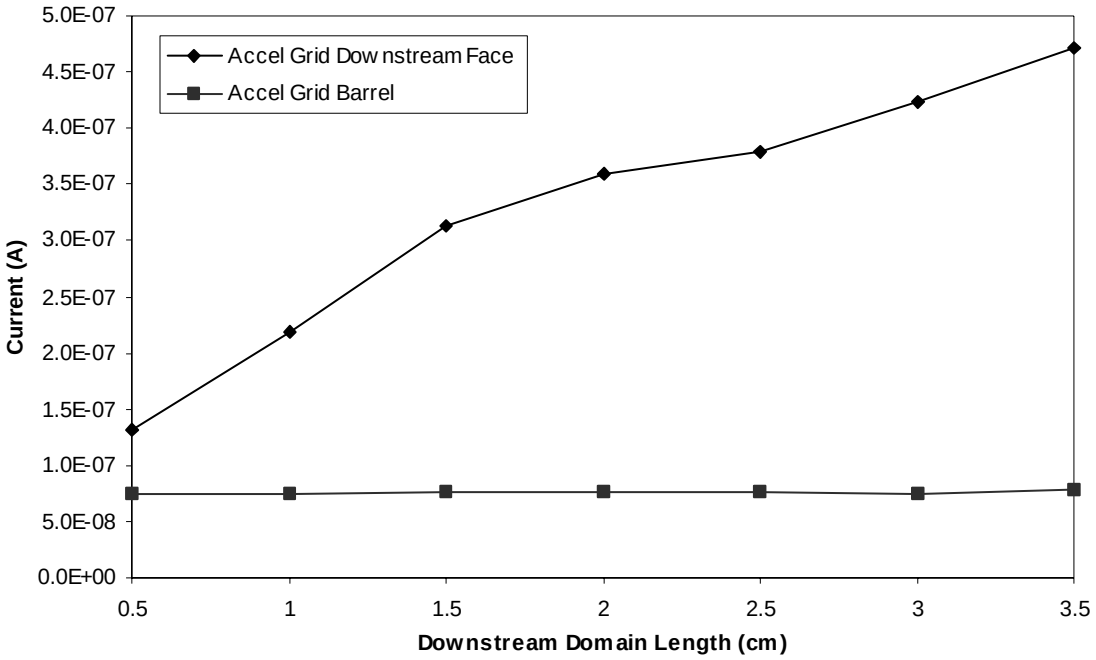

Figure 2. Change in accelerator grid current collected on the downstream face of the grid and the aperture wall as a function of domain length downstream of the ion optics.

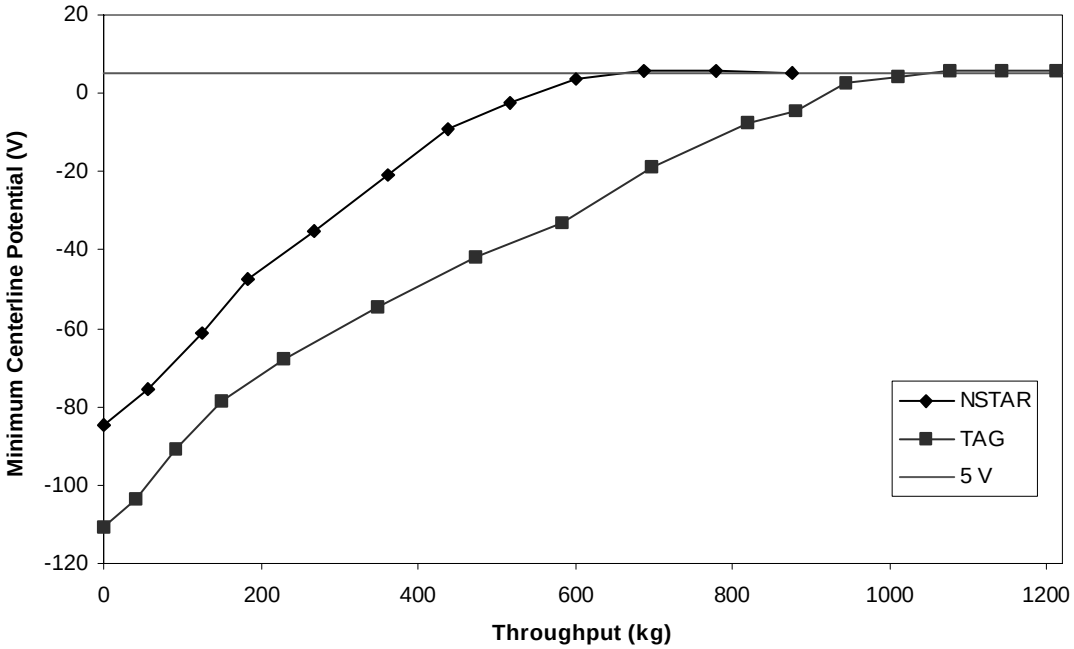

Figure 3. Electron backstreaming prediction for the 3.1 A operating point as a function of total thruster propellant mass throughput. When the minimum centerline potential reaches 5 V, electron backstreaming will occur.

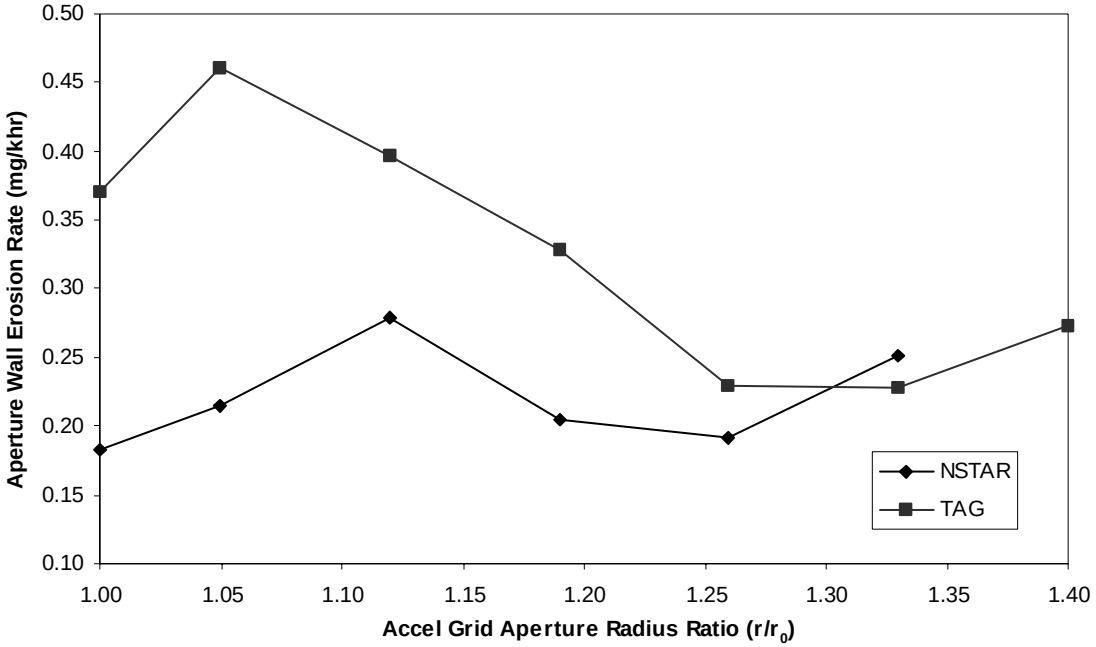

Figure 4. Accelerator grid aperture wall erosion rate as a function of aperture radius. The erosion rate for both sets of optics increases before dropping as the radius increases.

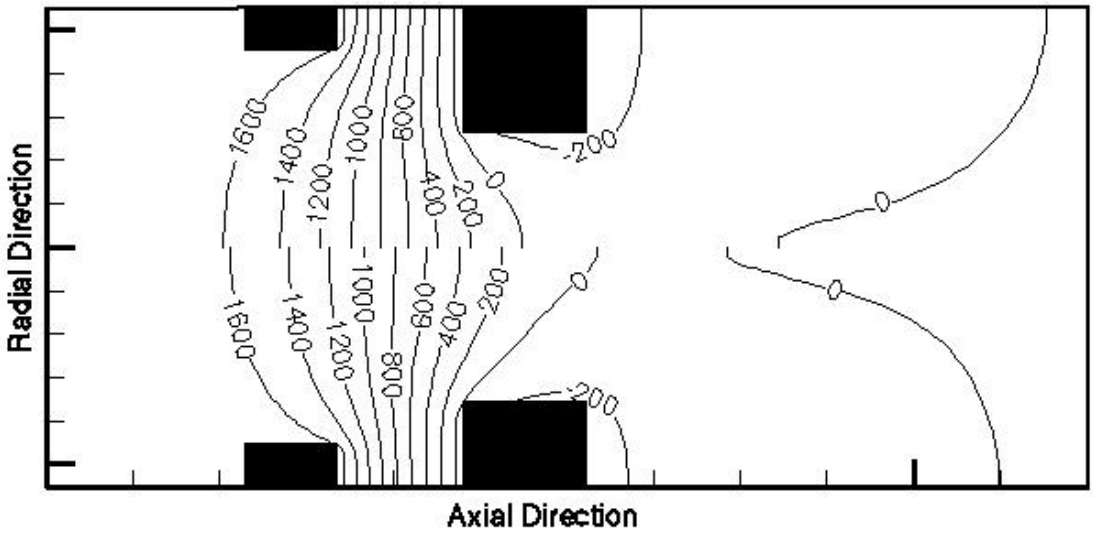

Figure 5. Potential contours for NSTAR optics, with values in Volts. The top half represents the optics at beginning-of-life, while in the bottom half the accelerator grid aperture diameter has increased by 40% due to erosion.

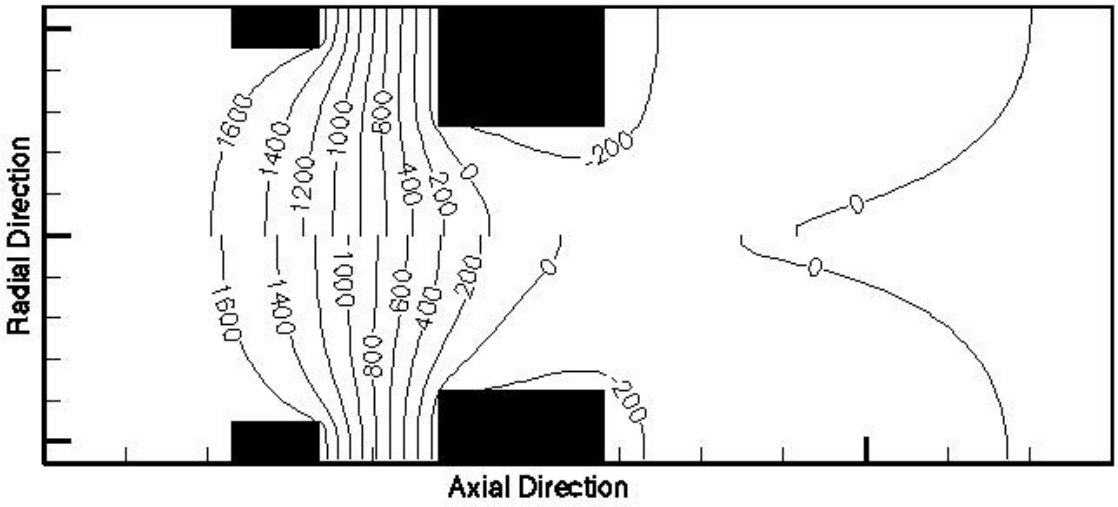

Figure 6. Potential contours for TAG optics, with values in Volts. The top half represents the optics at beginning-of-life, while in the bottom half the accelerator grid aperture diameter has increased by 33% due to erosion.

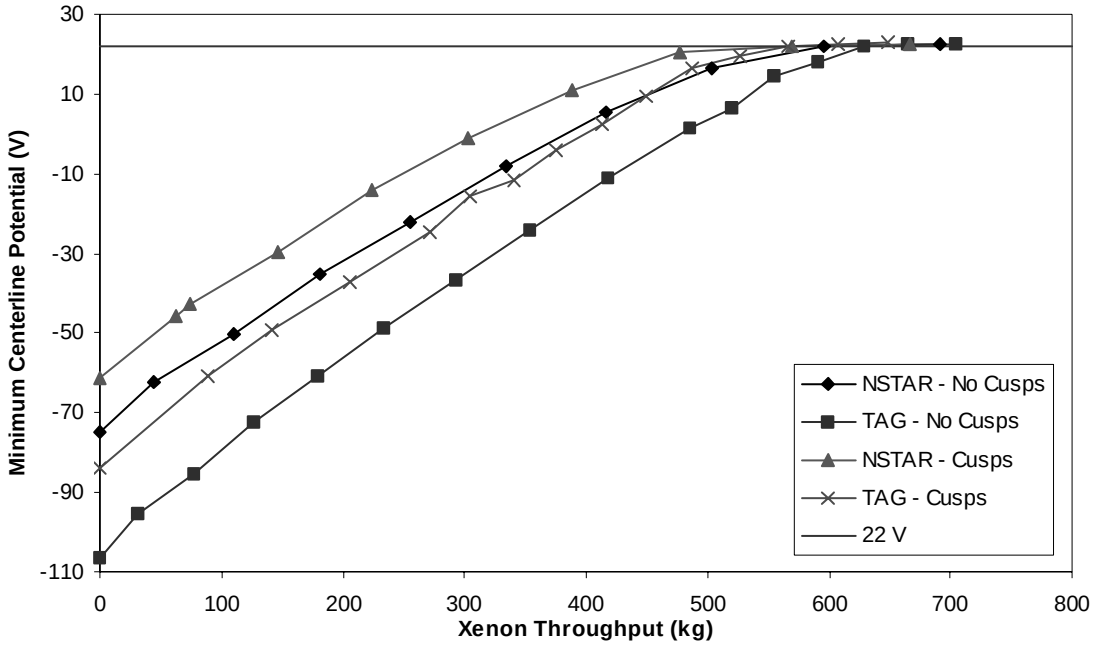

Figure 7. Minimum centerline potential as a function of Xenon mass throughput at the 3.52 A operating point, for both NSTAR and TAG optics, with and without cusped geometry. The downstream plasma is at 22 V for these operating points, so electron backstreaming occurs when the minimum centerline potential reaches that magnitude.

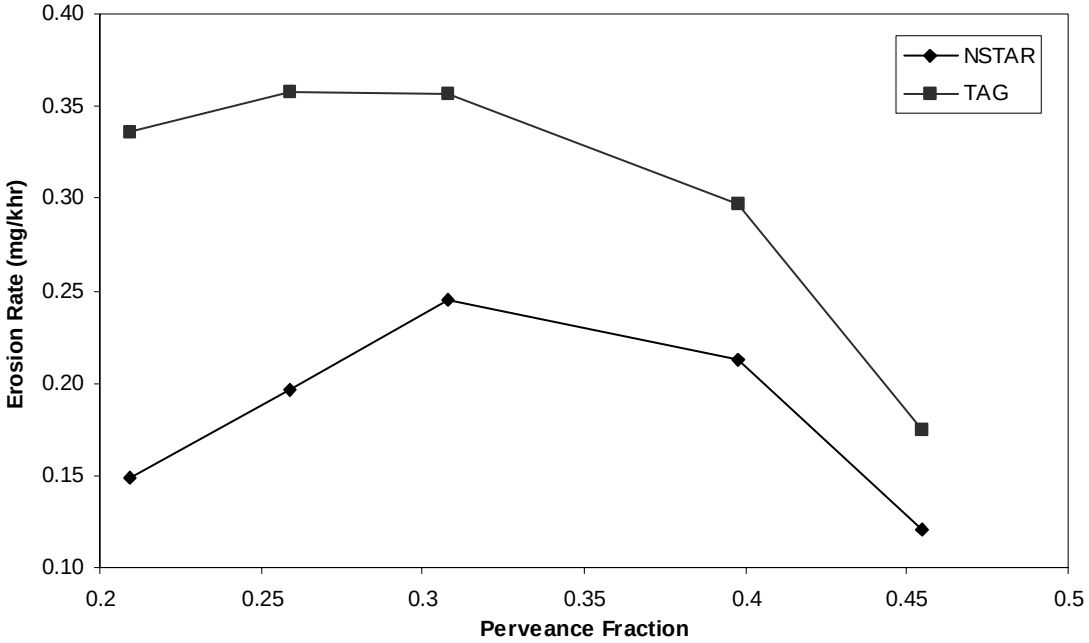

Figure 8. Erosion rate in mg/k-hr as a function of perveance fraction.

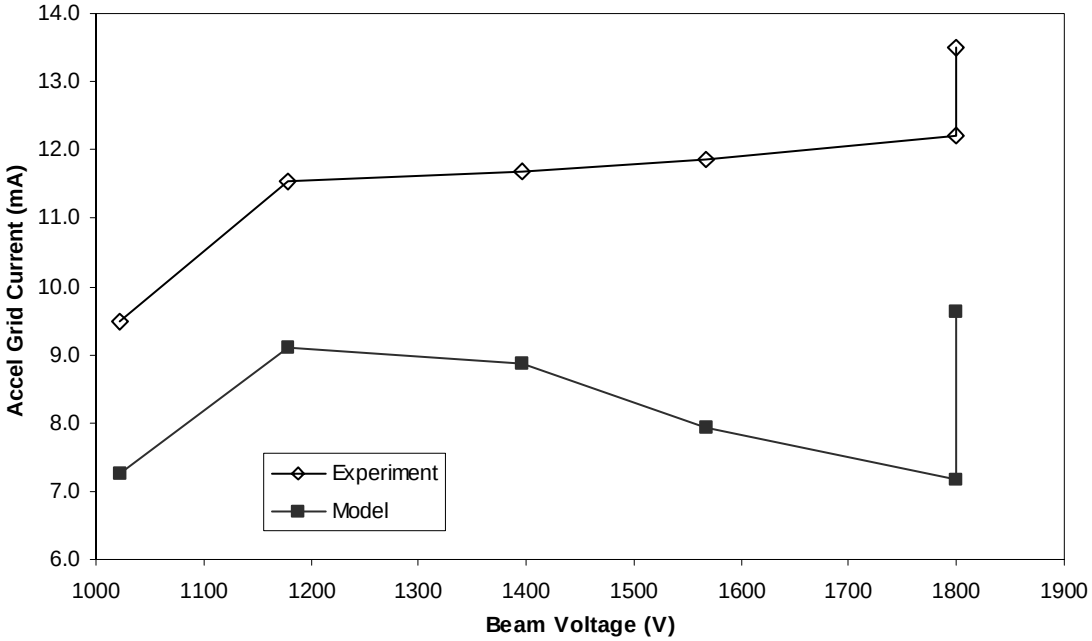

Figure 9. Comparison of experimental data for total accelerator grid current to simulation results, as a function of beam voltage.

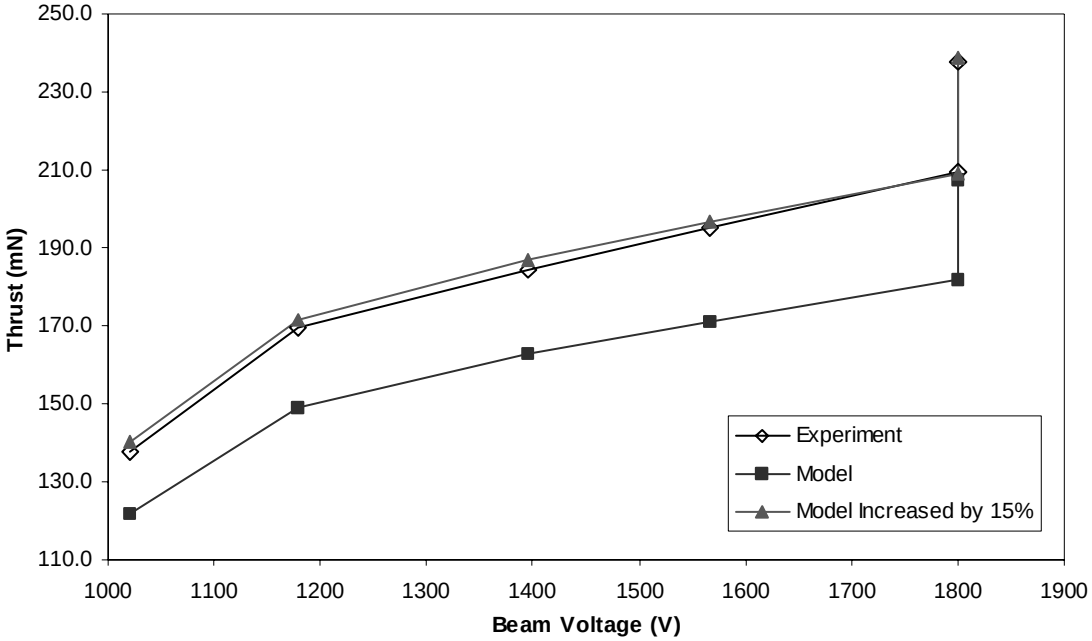

Figure 10. Comparison of experimentally measured thrust to simulation results, as a function of beam voltage. When the model results are increased by 15%, the comparison is almost exact.

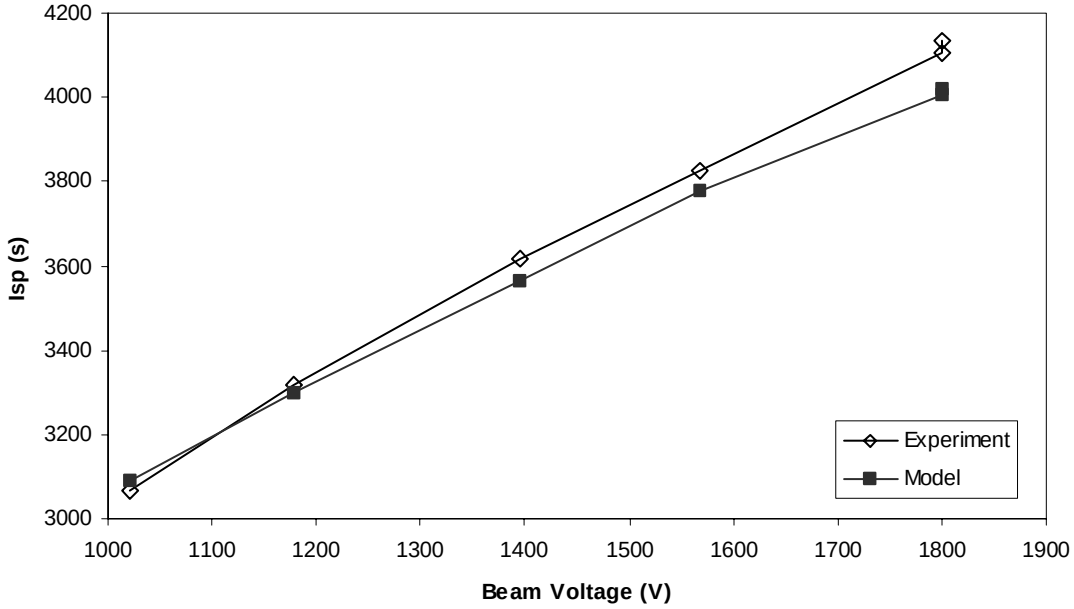

Figure 11. Comparison of experimentally measured specific impulse to simulation results, as a function of beam voltage.